Journal of Medicinal and Chemical Sciences 6 (2023) 376-391

Journal of Medicinal and Chemical Sciences

Journal homepage: http://www.jmchemsci.com/

Original Article

Preparation, Characterization, and Ninhydrin Removal by Al_2O_3 and V_2O_5 Nanoparticles

Zainab J. Abdul-Zahra*, Rashed T. Rasheed

Applied Chemistry Division, School of Applied Science, University of Technology, Baghdad, Iraq

ARTICLE INFO

Article history

Receive: 2022-05-08
Received in revised: 2022-06-13
Accepted: 2022-08-17
Manuscript ID: JMCS-2208-1619
Checked for Plagiarism: **Yes**
Language Editor:
Dr. Fatimah Ramezani
Editor who approved publication:
Dr. Zeinab Arzehgar

DOI:10.26655/JMCHEMSCI.2023.2.18

KEYWORDS

Ninhydrin
Al_2O_3
V_2O_5
Nanoparticles

ABSTRACT

Two nanoparticles, aluminum dioxide (Al_2O_3) and vanadium pentoxide (V_2O_5) were prepared by hydrothermal autoclave and reflex methods, respectively. Every nanoparticle was heated at two temperatures (90 °C and 400°C). The structures and surface morphology of these nanoparticles were characterized by FT-IR and UV/Visible measurements, X-ray diffraction (XRD), atomic force microscope (AFM), and scanning electron microscopy (SEM). The ninhydrin removal was measured for these nanoparticles. The results showed vanadium pentoxide has a higher ninhydrin removal activity in both cases (90 °C and 400 °C) than the aluminum oxide and the nanoparticles heated at 400 °C have more ninhydrin removal activity than the nanoparticles heated at 90 °C.

GRAPHICAL ABSTRACT

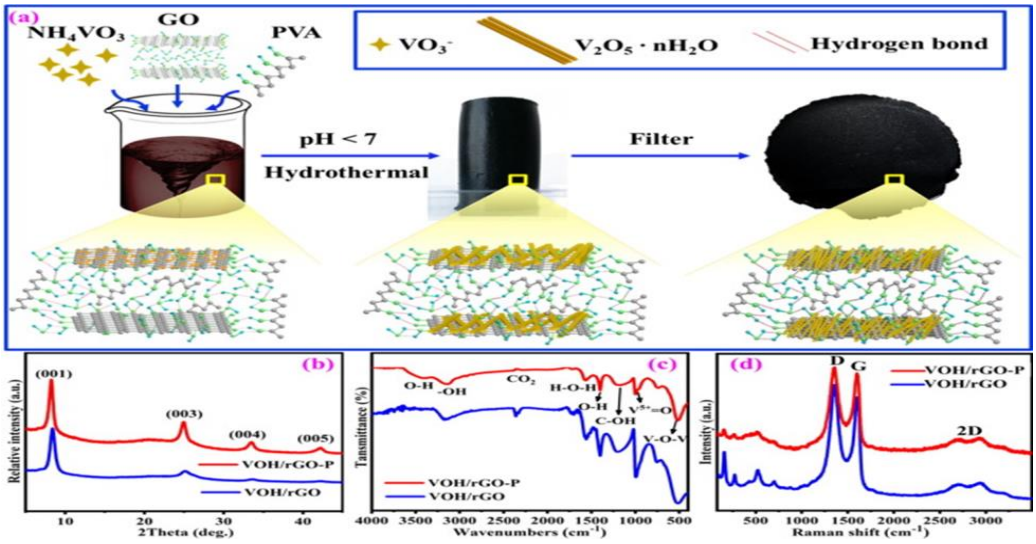

* Corresponding author: Rashed T. Rasheed
✉ E-mail: Email: Rashed.T.Rasheed@uotechnology.edu.iq

Introduction

Water is a necessary component for life and a valuable resource for modern existence [1]. Current global difficulties, including environmental contamination and a lack of energy supplies [2] have created serious problems for human populations on both the social and economic levels [3]. The main environmental factor contributing to illness and the early death in the world today is pollution [4]. People who consume dye-polluted water may experience a variety of health issues, including respiratory issues, nausea, skin rashes, allergic dermatitis, vomiting, dizziness, and even cancer [5]. Oil spills, toxic gases [6], heavy metals, pesticides, and organic compounds are just a few examples of many concerning contaminants [7]. It is necessary to create novel technologies and environmentally friendly practices. Nanotechnology is a promising technology because it has a better treatment efficiency [8] which allows for cost effectiveness with some restrictions and as a tolerable therapy method for contaminants [9]. For the treatment of waste or wastewater, nanoparticles have special qualities like high specific surface area, reactivity towards contaminants, high functionalization, and adsorbing abilities [10]. In this work, we try to use ammonia for the ninhydrin adsorption from aqueous solutions by using nano-oxides (V_2O_5 and Al_2O_3), prepared by the hydrothermal method.

Ninhydrin was discovered in 1910 by the English chemist, Siegfried Rohmann (1859 - 1943). In the same year, Ruhemann observed the ninhydrin circulation with amino acids [11]. Ninhydrin $C_9H_6O_4$ (2,2-dihydroxyindane-1,3-dione) is a high-melting-point organic compound with two hydroxyl groups on the same carbon atom [12]. Ninhydrin is a physiologically active chemical molecule found in abundance throughout nature. The chemical ninhydrin interacts with the amino group extremely quickly [13]. Ammonia as well as primary and secondary amines are all detectable with the help of the substance ninhydrin. A dark blue or purple color known as Riemann's purple is created with these free amines [14]. Ninhydrin is a potential chemical reagent used in various domains (e.g., chemical sciences, forensic investigations, bio-analytical work, and so on). Because of its low cost, easy availability, and strong reactivity, ninhydrin holds a prominent role in the chemical landscape. The presence of three consecutive electron-withdrawing carbonyl groups attached to the benzene ring makes the molecule structure particularly intriguing. It can make colored compounds because of its capacity to produce them [15]. In this work, nanoparticles of aluminum dioxide (Al_2O_3) and vanadium pentoxide (V_2O_5) were prepared by hydrothermal methods and the percentage of ninhydrin removal from aqueous solutions was measured and the optimum conditions were found.

Materials and Methods

Ammonium hydroxide (NH_4OH) and ammonium metavanadate (NH_4VO_3) were purchased from Sigma (Sigma–Aldrich, Taufkirchen, Germany). Likewise, nitric acid (HNO_3) (Alpha Chem), urea (NH_2CONH_2) was purchased from (Merck, Germany), cetyltrimethyl ammonium bromide (CTAP) was purchased from (BDH), and aluminum chloride hexahydrate ($AlCl_3.6H_2O$) from Sigma (Sigma–Aldrich, Taufkirchen, Germany).

Preparation of Aluminum Oxide Nanoparticles (Al_2O_3 NPS)

Aluminum oxide was prepared by using a hydrothermal method (autoclave). This could be done via aluminum chloride, cetyltrimethylammonium bromide (CTAB), urea (NH_2CONH_2), starting by dissolving 3 g (12.44 mmol) of aluminum chloride in distilled water (50 mL), and dissolving 1.25 g (20.833 mmol) of urea in distilled water (50 mL), dissolving 1 g (2.74 mmol) of cetyltrimethylammonium bromide (CTAB) in distilled water (50 mL), separately. Next, these solutions were mixed and stirred with a magnetic stirrer for 15 minutes. The homogeneous mixed solution was put into a teflon lined autoclave. The autoclave was then put into the furnace to be heated at 200°C for 6 hours and the white precipitate was washed three times with distilled water. After that, the precipitate was dried at 90 °C for 60 minutes, followed by 120 minutes of annealing at 400 °C [16], as demonstrated in the following equations:

$$NH_4\,C0\,NH_4\ + 3H_2O\ \rightarrow 2NH_4OH + CO_2 \quad (1)$$

$$AlCl_3.6H_2O + 3\,NH_4OH \rightarrow Al(OH)_3 + 3NH_4Cl\ + 6H_2O \quad (2)$$

$$2Al(OH)_3 \xrightarrow{400℃} Al_2\,O_3\ + 3H_2O \quad (3)$$

Creation of Nanoparticles (V_2O_5)

The hydrothermal (reflex) technique of producing vanadium pentoxide involves dissolving two grams (1.704 mmol) of ammonium metavanadate (NH_4VO_3) in a 70:30 mixture of distilled water and ethanol. Next, 0.2 g (0.548 mmol) of cetyltrimethylammonium bromide (CTAB) and a few drizzle of HNO_3 nitric acid were added to it till the pH is 2.5, and then it was put in an autoclave for 12 hours at 200 °C, washing it numerous times, drying it at 90 °C. After that, it was annealed for two hours at 400 °C [17], as indicated in the following equations:

$$2NH_4VO_3 + 2HNO_3 + nH_2O \xrightarrow[CTAB]{CH_3CH_2OH} V_2O_5nH_2O + 2NH_4NO_3 + \ H_2O \quad (4)$$

$$V_2O_5nH_2O \xrightarrow{90\,°C} V_2O_5.1.8H_2O + (n-1.8)H_2O \quad (5)$$

$$V_2O_5.1.8H_2O \xrightarrow{500°C} V_2O_5 + 1.8H_2O \quad (6)$$

Adsorption of ninhydrin pollutants

Ninhydrin was adsorbed from aqueous solutions by using the prepared nano-oxides in the case of preparation and solidification. The absorbance (%R) ninhydrin removal measurements were performed by the UV/Vis spectrometer approach at 508 nm wavelength as a procedure as follows: two 50 mL containers were filled up with a test (T) and a blank (B). Only 0.01 g of metal oxide (V_2O_5, Al_2O_3) was added to the T containers. By using a micropipette, each T and B container was filled up with 5.0 mL of carbonate buffer (pH=10). 0.25 mL of ninhydrin was added to the T and the B containers, and then all of these containers were shaken on a shaker for 15 minutes at 250 rpm. After the vibration period, the samples were centrifuged to separate them. 0.15 mL of ammonium hydroxide was added to all containers after 20 minutes and the absorbance was measured by an ultraviolet visible spectrophotometer at a wavelength of 508 nm.

The ninhydrin removal percentage (%R) can be calculated by differentiating the two (initial and final) concentrations divided by the initial concentration, as illustrated by the following equation 7 [18].

$$Percentage\ removal\ (\%R) = [(C_O - C_t)/C_0] \times 100 \quad (7)$$

Where, C_o is premier ninhydrin concentration (mg/L) and C_t indicates final ninhydrin concentration (mg/L).

The adsorbed amount of ninhydrin at equilibrium was calculated by using equation 8 [19, 20].

$$q_t = (C_o - C_t)\,{}^{v}/_{W} \quad (8)$$

Where, V indicates the volume of ninhydin solution (mL), W, the weight of nanoparticles (g), and q_t = adsorption capacity of ninhydrin.

Optimum condition

The ninhydrin contaminant was absorbed by the following nano-oxides (V_2O_5 and Al_2O_3) in both cases (as prepared and annealed), where the identical weight (0.01 g) and volume (5.4 mL) of each generated nanoparticle were utilized. The results indicated that vanadium pentoxide (as prepared) is the best nanoparticle to deliver the highest efficiency of ninhydrin pollution, as displayed in Figure 8.

Optimum condition of V_2O_5 -as to the adsorption of ninhydrin pollutants

Preliminary research was done to determine the best conditions for nihydrin adsorption:

A. The effect of weight

The effect of weight on ninhydrin elimination was investigated. Initially, various weights of

vanadium pentoxide (V_2O_5 -as) (0.010, 0.0150, 0.020, 0.025, and 0.030) g were taken. Following that, ninhydrin (250 M) and a buffer solution (5 mL) are added to all weights. The solution is shaken for 15 minutes at 250 rpm, the solution is filtered and finally, ammonia (150 M) is added and combined. A final volume of 5.4 mL was measured at room temperature and the absorbance was measured with a spectrophotometer. The experiment was carried out under the following conditions: reaction duration of 20 minutes, pH = 10, t= 25 °C NH_3 = 0.1122 M, and ninhydrin 0.2245 M.

B. The effect of ninhydrin concentration

The effect of concentration was studied on ninhydrin removal. Initially, different concentrations of ninhydrin (25, 50, 75, 100, 125, and 150) µM were taken, and then they were placed in containers, (5 mL) of buffer solution and vanadium pentoxide (V_2O_5) (0.015 g) were added. The solution was shaken for 15 minutes at 250 rpm, and then it was separated by filtration so ammonia (150) is added (µM) and mixed at room temperature in a final volume of 5.4 mL. The absorbance was measured by a spectrophotometer. The experiment was conducted while keeping other conditions constant such as reaction time of 20 min, pH = 10, t = 25 °C , V_2O_5 = 0.015 g, and ammonium = 0.112 M.

C. The effect of shake speed

The effect of shaking speed was investigated on the removal of ninhydrin. Initially, vanadium pentoxide (V_2O_5-as) was taken by weight (0.015 g), and then ninhydrin (200 µM) and a buffer solution (5 mL) were added. Next, the solution was shaken for 15 min at different shaking speeds (50, 100, 150, 200, and 250) rpm after which the solution was separated by filtration, and then ammonia (300 µM) was added and mixed at room temperature with a final volume of 5.4 mL. After that, a spectrophotometer was used to measure the absorbance. Other variables remained constant throughout the experiment, including the reaction duration of 20 minutes, pH=10, t=25 °C, V_2O_5 = 0.02 g, ninhydrin = 0.2245 M, and NH_3 = 0.1122 M.

D. The effect of shake time

The effect of shake time was examined on the ninhydrin removal. Initially, vanadium pentoxide (V_2O_5-as) was taken by weight (0.015 g), and then ninhydrin (100 µM) and a buffer solution (5 mL) were added. Next, the solution was shaken for different shaking times (5, 10, 15, 20, and 25) minutes at 150 rpm. After that, the solution was separated by centrifugation, and then ammonium (300µM) was added and mixed at room temperature with a final volume of 5.4 mL, by using a spectrophotometer, the absorbance was measured. Other variables were kept constant throughout the experiment, including reaction duration of 20 minutes, pH =10, t= 25 °C , V_2O_5 = 0.015 g and ninhydrin = 0.2245 M, and NH_3 = 0.1122 M.

Results and discussion

Optical properties of the nanoparticle solutions

The optical characteristics of nanoparticle solutions are discussed. By dissolving metal oxides in ethanol, the optical properties of nanoparticle solutions (approximately 1x 10^{-5} M) were created. The optical prosperity (transmittance) of metal oxides is between 90 °C and 400°C, with wavelengths extending from 250 nm to roughly nm. The following equation can be used to calculate the value of the energy gap:

$$Energy\ gap(eV) = \frac{1240}{\lambda \max} \qquad (9)$$

Where, λ is the maximum transmittance in nm and 1240 is the conversion factor used to convert nm into eV [21]. The spectrum of Al $(OH)_3$ as prepared in Figure (1a), illustrates the transmittance border that has moved to a higher wavelength (redshift) from 278 nm to 299 nm, the higher optical transmittance was seen as annealing temperatures increased, which was attributed to structural uniformity and particle crystallization. The energy gap of Al $(OH)_3$ as-prepared is 4.4 eV as a consequence of equation 9. While Al_2O_3 annealing at 400 °C results in 4.1 eV, this result agrees with the reference [22]. While the vision of (V_2O_5) as prepared in Figure 1b appear annealing temperature was increased, the transmittance border shifted to a lower wavelength (blue shift) from 520 nm to 412 nm. The energy gap of

prepared $V_2O_5.nH_2O$ is 2.3 eV, while annealing at 400 °C (V_2O_5) is 3.0 eV. These findings are in agreement with those in [23].

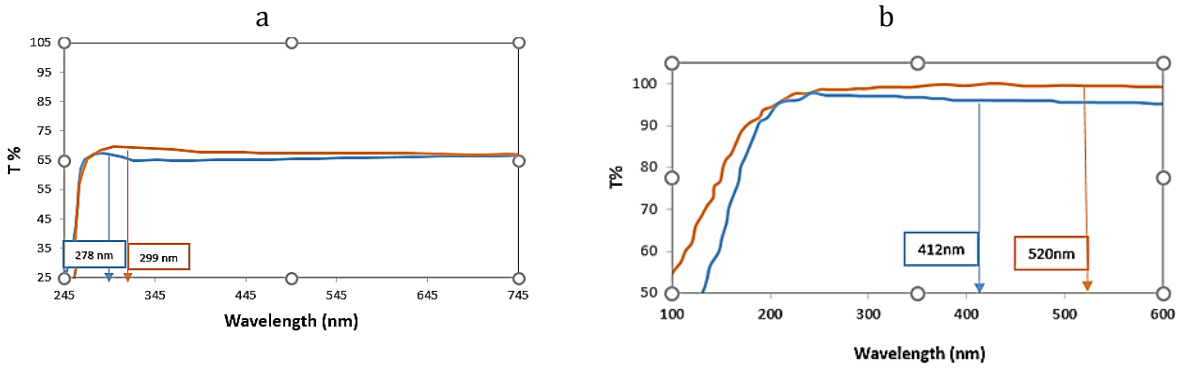

Figure 1: The visual transmittance for nanoparticles, (a) Al_2O_3, and (b) V_2O_5 annealing at different temperatures (90 °C and 400 °C)

The FTIR spectrum

FTIR spectra for Al (OH) $_3$ with Al_2O_3 nanoparticles

FTIR spectroscopy was used to determine the quality and type of alumina nanoparticles produced by the hydrothermal method. The FTIR spectrum of $Al(OH)_3$ is shown in Figure 2a (as prepared). Broad band can be given to the expansion and curvature vibrations of water molecules in the sample about 3289 cm^{-1} and 1665 cm^{-1} [24], water deformation vibrations were also responsible for the peak at 1540 cm^{-1} [25]. Meanwhile, water deformation vibrations were further responsible for the peak at 1420 cm-^{1}. The Al–O vibration mode causes a band to form at 1180 cm^{-1}, which is typical for γ-alumina. The band at 619 cm^{-1} is generated by the Al-O-Al bond in the gamma phase of alumina. The peak at 746 cm^{-1} is attributed to Al-O bond bending vibrations. FTIR spectrum of samples annealing at 400°C. Figure 2b show the broad band at 3485 cm^{-1} is corresponded to -OH stretching vibration and the band at 1639 cm^{-1} is corresponded to the observed physisorbed water [26]. The band from 840- 520 is corresponded to functional groups of (O-Al-O) bonds [27].

FTIR Spectra $V_2O_5.nH_2O$ and V_2O_5 nanoparticles

Figure 2c illustrates the FTIR spectrum of V_2O_5 nanoparticles (as prepared) $V_2O_5.nH_2O$ heated at 90 °C for 60 minutes. The O-H stretch and bend are demonstrated by a broad band at 3230 cm^{-1} and a peak at 1655 cm^{-1}, respectively. The peak at 1482 cm^{-1} is due to the CTAB-related bending vibration of C=C, The distinctive peaks of vanadium pentoxide for $V_2O_5.1.8H_2O$ nanoparticles at 968 cm^{-1}, 731 cm^{-1}, 532 cm^{-1}, and 494 cm^{-1} appear to be corresponded to the vibrations of V=O, V-O-V symmetric, and V-O-V asymmetric, meanwhile V-O stretching peak is observed at 459 cm^{-1} [28]. Figure (2d) depicts the annealing of V_2O_5 at 400 °C for 120 min., The V=O stretching vibration is allocated to the band at 1020 cm^{-1}, while the V-O-V deformation mode is assigned to the band at 810 cm^{-1} [29]. The bands at 554-430 is corresponded to the asymmetric and symmetric stretching vibrations of triply coordinated oxygen (chain oxygen) bonds [30].

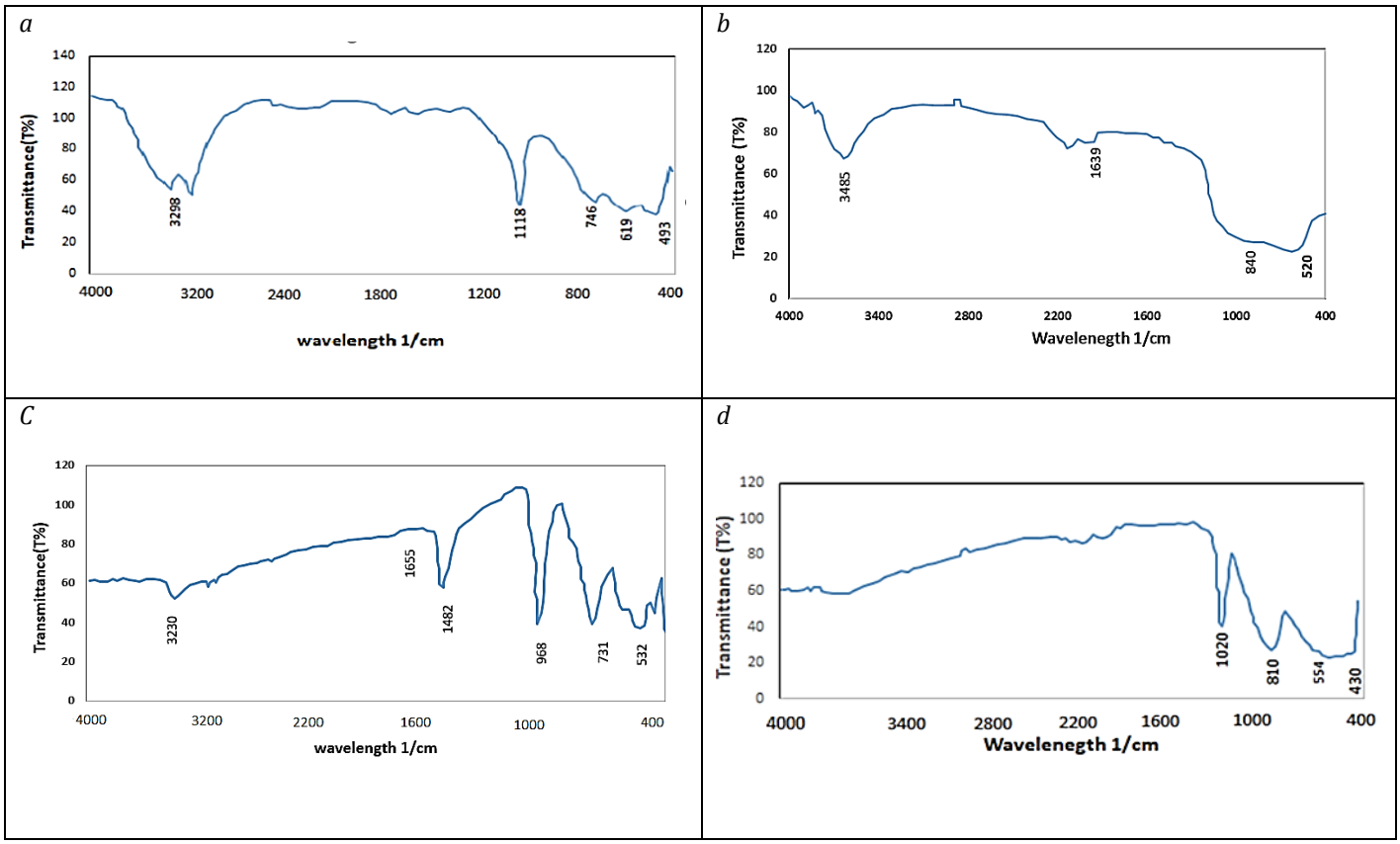

Figure 2: FTIR analysis of Al_2O_3 (a) as prepared, (b) heating at 400 °C and V_2O_5, (c) as-prepared, and (d) heating at 400°C

XRD diffraction analysis

The X-ray diffraction patterns for Al (OH) ₃ and Al_2O_3 nanoparticles

The X-ray diffraction (XRD) of Al_2O_3 was used as prepared measurements to verify the sample's crystal structure and phase composition. That is prepared through the hydrothermal method. The indexed peaks and the recorded diffraction pattern are illustrated in Figure (3a). Three distinct peaks are (120), (031), and (002) were detected at 2θ = 28.26, 38.41, and 49.10, respectively related to γ-AlOOH, acorrding to (JCPDS card No. 21-1307) [31]. The XRD pattern of the Al_2O_3-NPs after annealing at 400 °C revealed that the sample was in cube crystal symmetry, with the central lattice of the face figure (3-b) for the XRD pattern, the computed network parameter was 7.901 A°, that was the value of the powder diffraction standards ICDD card. The observed values are consistent with the Joint Commission Standard (00-056-0457). The planes of (311), (222), (400), (511), and (440) are corresponded to the measured peaks for Al_2O_3 at (2θ = 37.03, 39.34, 45.90, 61.16, and 66.98°). The nanoparticles were mostly gamma-phase, with two major diffraction intensity peaks at 2 = 45.90o and 66.98o, respectively. The peak at 2θ = 37.03 for the nanocomposite consists of one peak, matching the Al_2O_3 (311) peak at 2θ = 37.03 [32]. The Debye-Scherer formula, which is given, is used for calculating crystallite size by FWHM of diffraction peaks [33].

$$D = K\lambda/\beta cos\ \theta \qquad (10)$$

Where, D denotes the size of the crystallite, and (k) the form factor (0.98), ƛ is the wavelength of X-ray, (β) is the line boarding at a half-maximum intensity (FWHM) of an individual peak at 2Θ (where Θ is the Bragg angle) [34].The average grain size of Al_2O_3 nanoparticles was obtained by using the Scherer equation (10) and the lattice constants (a), (b), and (c) of γ-AlOOH and (a) of Al_2O_3 Nanoparticles were calculated as demonstrated in Table (1) and equations (11) and (12), respectively.

$$1/d_{hkl}^2 = \frac{h^2}{a^2} + \frac{k^2}{b^2} + \frac{I^2}{c^2} \qquad (11)$$

$$1/d_{hkl}^2 = (h^2 + k^2 + I^2)/a^2 \quad (12)$$

Where, (d) is the spacing parameter distance, (hkl) Miller indices, (a, b, and c) are the lattice constants.

The X-ray diffraction patterns for $V_2O_5.nH_2O$ and V_2O_5 nanoparticles

The XRD consequence for V_2O_5 prepared by the hydrothermal method (reflex) at different temperatures as prepared at (90°C and annealing at 400°C) are illustrated in Figures (4a) and (4b). The major peak as the most noticeable one is 2θ = (40.96, 44.94, and 47.79) which is corresponded to the diffraction values of (002), (411), and (600). This could be related to $V_2O_5.nH_2O$, which is corresponded to VOOH at 2θ = 27.8 based on the card's unique identification number (JCPDS card No. 01-089-0612)[35]. The primary diffraction peaks of 2θ = (20.35, 21.78, 31.08, 32.04, 34.38, 51.0, and 61.15) are correlated to the typical diffraction of the V_2O_5 planes (010), (101), (301), (011), (310), (020), (321). Match is a diffraction peak. The diffraction peaks are consistent with the V_2O_5 pattern (JCPDS card no. 41-1426). The diffraction peaks might be attributed to an orthorhombic structure of the V_2O_5 phase with lattice values a = 11.46 °A, b = 3.55°A, and c = 4.359 °A [17]. The size of crystal particles can be calculated by using the Scherer equation 10. The obtained lattice constants show that the nanocrystal belongs to the orthorhombic system Equation 11 and Table 2.

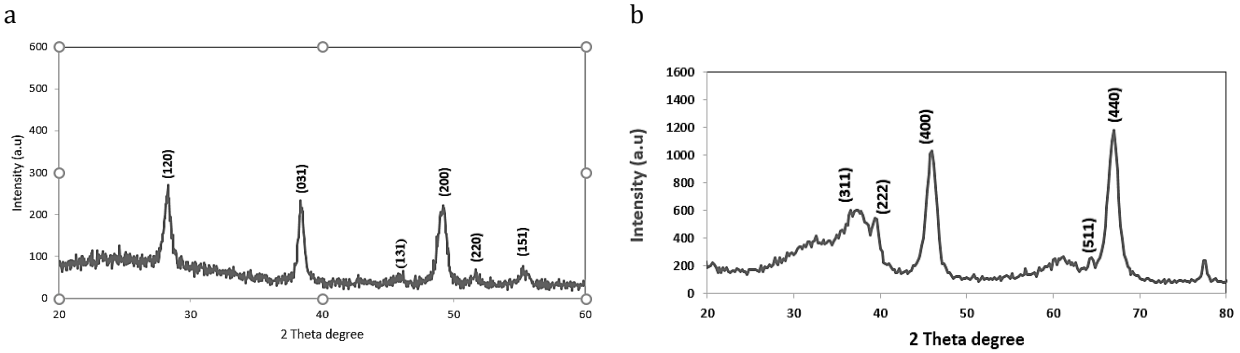

Figure 3: (a) XRD of Al (OH) $_3$ heating at 90 °C for 60 min, and (b) XRD of Al_2O_3 heating at 400 °C for 120 min

Table 1: The results of the XRD for aluminum oxide at 90°C and at 400°C for 120 min

Aluminum oxide heated at	2θ (deg)	hkl	FWHM (deg)	d (A°)	D (A°)	Lattice constant (A°)		
						a	b	c
90 ˚C for 60 min	49.106	200	0.80500	1.85375	108.4	3.707	12.016	2.90
	38.413	031	0.58890	2.34148	134.8	-	-	-
	28.263	120	0.66760	3.15495	122.7	-	-	-
400 ˚C for 120 min	66.89	440	1.54320	1.39750	61.66	7.901	7.901	7.901
	45.90	400	1.44790	1.97537	54.83	-	-	-
	37.03	311	4.45720	2.42535	18.81	-	-	-

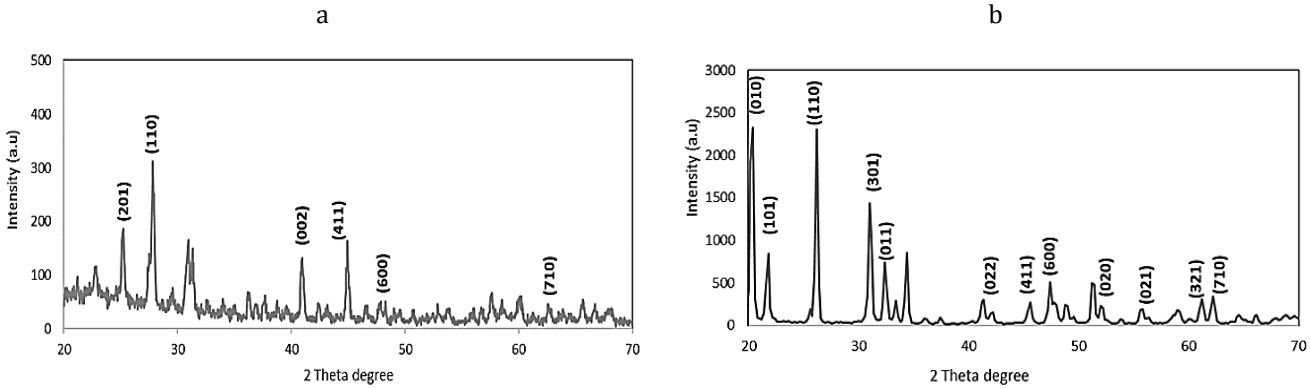

Figure 4: (a) XRD of $V_2O_5.nH_2O$ heating at 90 °C for 60 min, and (b) XRD of V_2O_5 heating at 400 °C for 2 hours

Table 2: The consequence of the XRD for V_2O_5 at 90 °C for 60 min, and at 400°C for 120 min

Vanadium pentoxide heated at	2θ (deg)	hkl	FWHM (deg)	d (A°)	D (A°)	Lattice constant (A°)		
						a	b	c
90 ◦C for 60 min	27.88	110	0.29050	3.19742	281.66	11.42	3.34	4.40
	25.24	201	0.28890	3.52537	281.66	-	-	-
	44.94	411	0.27470	2.01523	313.8	-	-	-
400 ◦C for 120 min	20.35	010	0.53200	4.35926	151.6	11.46	3.55	4.359
	26.21	310	0.46420	3.39626	175.6			
	31.08	011	0.51210	2.87473	160.9			

Surface morphology by atomic force microscopy (AFM)

Aluminum oxide (Al_2O_3) nanoparticles

Figures (5a and 5b) display the AFM pictures of Al_2O_3 produced, annealed at various temperatures, aluminum oxide nanoparticle dispersion, and accumulation change from bubbles (Figure 5a) to uniform morphologies (Figure 5b). This could be connected to the conversion of most hydroxides $Al(OH)_3$ into oxides (Al_2O_3) during high-temperature heating (400°C), As seen in Table (3), the average grain size increases from 38.656 nm (as prepared) to 53.82 nm (annealing). This could be due to the sample requiring less heat to convert all hydroxide into oxide.

Vanadium pentoxide (V_2O_5) nanoparticles

Figures (6a a and 6b) depict A FM pictures of V_2O_5 produced and annealed at various temperatures (90 °C and 400°C). According to the findings, nanoparticle dispersion and accumulation appear to be huge balls (Figure 6a) that are reduced to smaller sizes when annealed at 400 °C (Figure (6b)). These results are related to the temperature effect on the water molecules loss from the sample as in the following neutralization:

$$V_2O_5.nH_2O \rightarrow V_2O_5 + nH_2O \qquad (13)$$

These consequences are in accordance to the average grain size determined by AFM analysis, which, as listed in Table 3, changes from 40.46 nm of ($V_2O_5.nH_2O$) to 41.07 nm of V_2O_5 as the temperature increases from 90 °C to 400 °C.

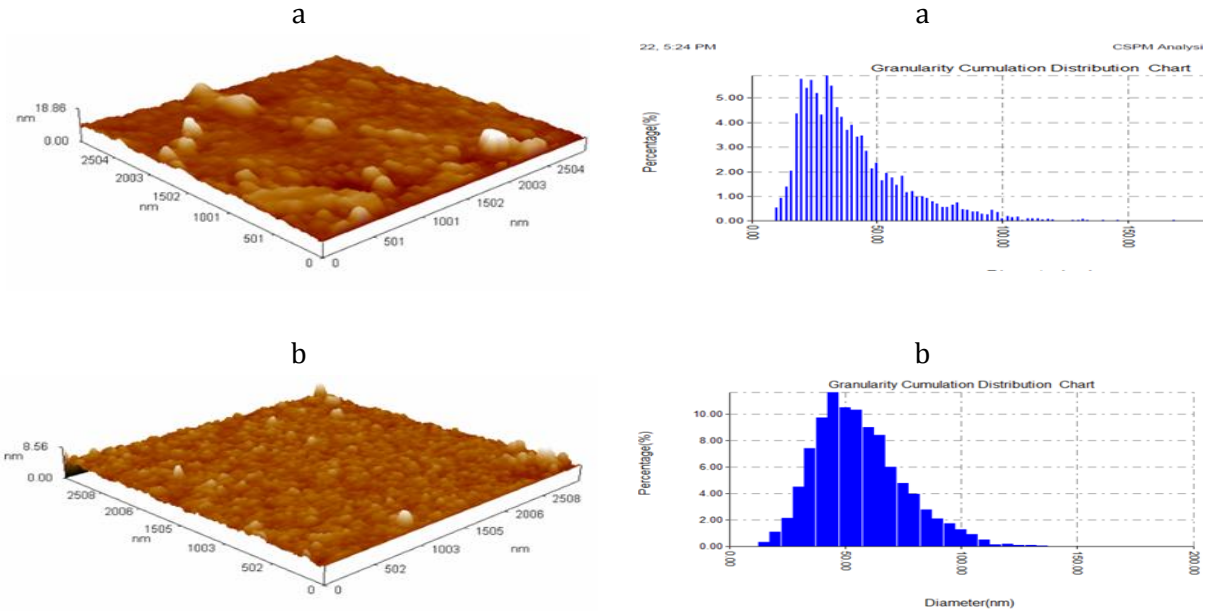

Figure 5: Atomic force microscopy pictures in three diminution and granularity collection division charts of Al_2O_3 at different temperatures: (a) 90 °C for 1 hour, and (b) 400 °C for 2 hours

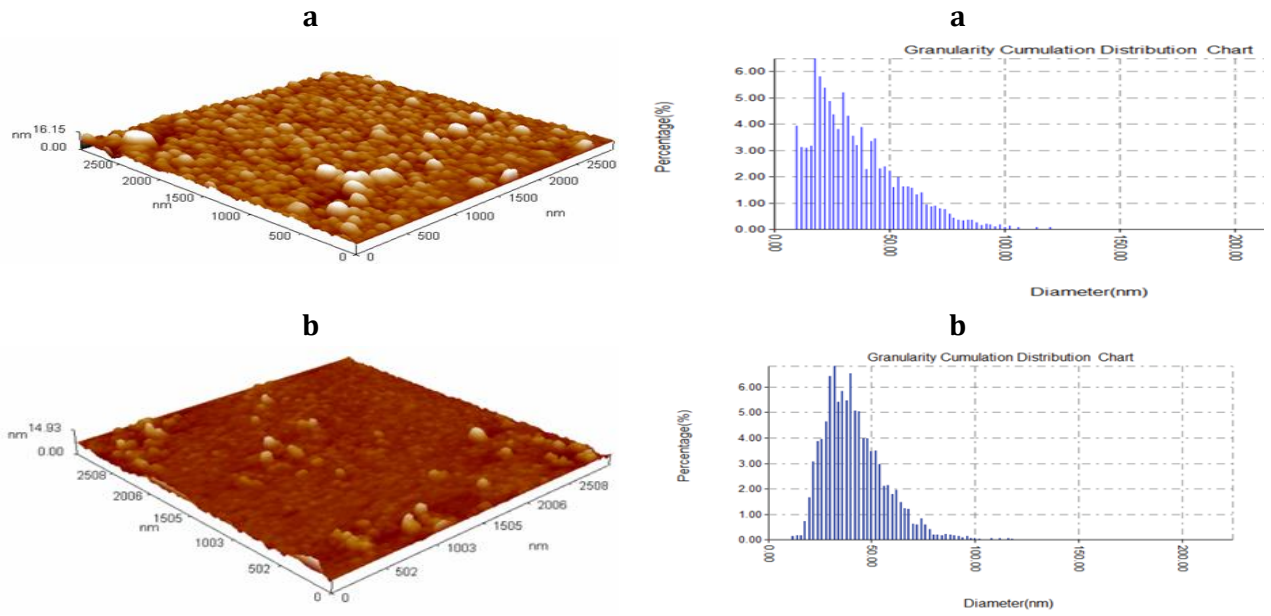

Figure 6: Atomic force microscopy pictures at three demotion and granularity collection division charts of a V_2O_5 at different temperatures: (a) 90 °C for 1 hour, and (b) 400 °C for 2 hours

Table 3: Variation of grain size for pure V_2O_5, Al_2O_3 at (90 °C and 400°C)

Sample	Average grain size (nm)		Ionic potential (Charge/radius)
	As prepared (90 °C)	Annealing (400 °C)	
Al_2O_3	38.65	53.82	0.044
V_2O_5	40.46	41.07	0.073

Surface morphology by Surface Scanning Electron Microscopy (SEM)

The SEM surface morphological image at a magnification of 500 nm and its findings for metal oxide nanoparticles (Al_2O_3 and V_2O_5) were provided by the hydrothermal technique and heated at 400 °C for 2 hours, as displayed in Figure (7). These analyses show a high porosity structure emerged on the surfaces of the sample by increasing annealing temperature. On the surface, clusters of nanoparticles were seen, with a few aggregates. Figure (7a) shows the SEM image of the annealed Al_2O_3 nanoparticles with the formation of clusters, while Figure (7b) depicts the surface morphology (V_2O_5) resembles a Cubic's.

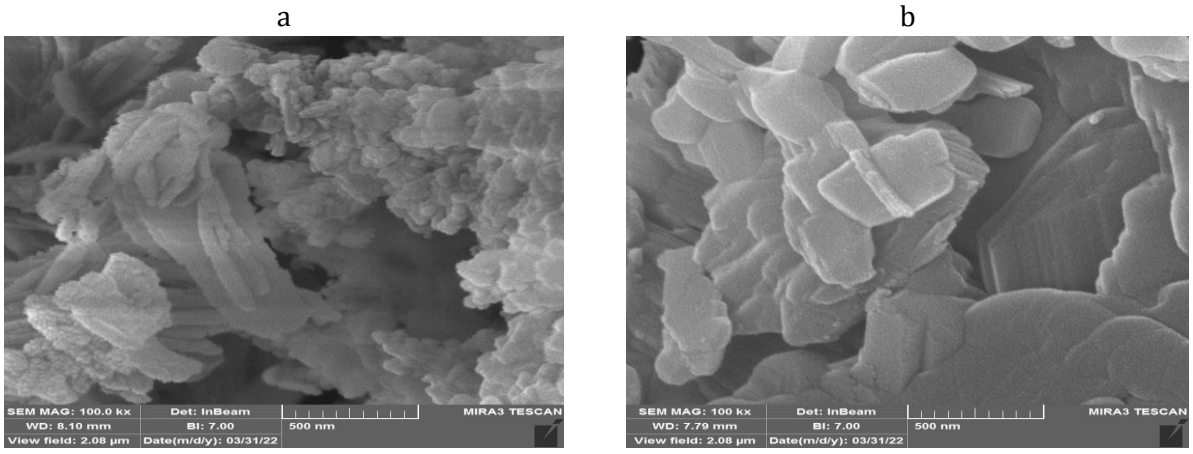

Figure 7: SEM image for (a) Al_2O_3, and (b) V_2O_5 annealing at 400 °C for 120 min

Applications

The adsorption of ninhydrin pollutants onto nanoparticles

Nanoparticles were used to adsorb pollutants from aqueous solutions, such as (ninhydrin contaminant) in carbonate buffer solution (50 mM, pH = 10) by using spectrophotometry technique at wavelength (λ = 508 nm), with ammonium hydroxide red indicator solution. Equation 7 was used to calculate the removal ratios (%R) of ninhydrin contaminants on the nanoparticles, while equation 8 was used to calculate the adsorption capacity of ninhydrin (q_t) contamination on nanoparticles.

The levels of ninhydrin percentage removal (%R) from aqueous solutions varied depending on the kinds of nanoparticles and the intensity of heating temperatures, according to the findings. For nanoparticles (as prepared), V_2O_5 has the largest ninhydrin %R of the nanoparticles, while Al_2O_3 has its lowest amount. The %R of nanoparticles in the as-prepared order was (V_2O_5 > Al_2O_3), while for nanoparticles (annealing), V_2O_5 has the highest ammonium %R. However, Al_2O_3 has its lowest amount. As depicted in Figure 8 and Table 4, the %R sequence of nanoparticles in the annealing order was (V_2O_5 > Al_2O_3). V_2O_5 (as prepared) shows a decrease in adsorption when ninhydrin is removed from aqueous solutions despite the increase in average grain size from (40.46 nm to 41.07 nm), which might be due to the collecting or interfere of the adsorption site. While adsorption to nanoparticles increases upon (annealing) at 400 °C may be connected to the presence of substantial bonding sites on the nanoparticles' surface area. Or it's high ionic, while the high rise in adsorption ninhydrin from aqueous solutions by Al_2O_3 from none (as-prepared) to the highest (annealing) could be attributed. This may be due to the highest surface area (the biggest grain size) that is not suitable for these nanoparticles (see Table 3).

Meanwhile, the results revealed that the adsorption capacity (q_t) of nanoparticles (heating at 90 °C), for ninhydrin pollutants was similar to the situations occurred in the %R process (at 90 °C) in the same sequence, and for samples annealed at 400°C. This resemblance is explained by the fact that all tests used the same quantity of contaminants and weight of nanoparticles, as listed in Table 4. V_2O_5 nanoparticles have the highest adsorption capacity (qt) compared with Al_2O_3 metal oxide.

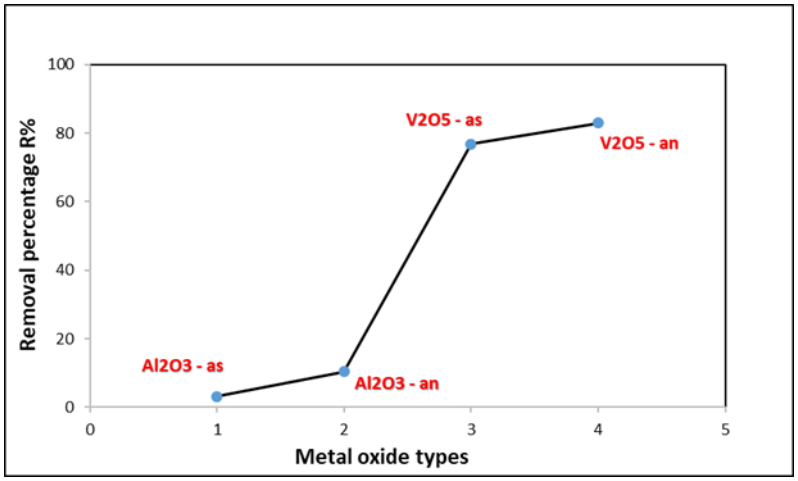

Figure 8: Adsorption of ninhydrin curve of nanoparticles at two (90 °C and 400 °C)

Table 4: The values of percentage removal (%R) and adsorption capacity (q_t) of ninydrin pollution on to nanoparticles (heating at 90 °C and 400 °C)

Metal Oxide type	Percentage removal (%R)		Adsorption capacity (q_t)	
	As-prepared	annealing	As-prepared	annealing
Al_2O_3	3.125	10.416	11.539	39.596
V_2O_5	76.736	82.986	294.585	318.579

Optimum condition of $V_2O_5.nH_2O$ to adsorption of ninhydrin pollutants

To determine the best conditions, different parameters were investigated such as initial weight of nanoparticles, initial concentration of ninhydrin, the effect of shake speed, and the effect of shake time.

A. The effect of weight

To determine the effect of vanadium pentoxide weight on ninhydrin removal pollutants different weights (0.01, 0.015, 0.020, 0.025, and 0.030) g of $V_2O_5.nH_2O$ were used to a fixed ammonium concentration (0.1122 M), ninhydrin concentration (0.2245 M), carbonate buffer (0.099 M), pH=10, shake speed (250 RPM), and shake time (15 min). Figure (9) and Table (5) illustrate the findings.

Table 5: The effect of the vanadium pentoxide weight on the values of percentage removal (%R) and adsorption capacity (q_t) adsorbent of ninhydrin pollution

	Weight (g)	Percentage removal (%R)	Adsorption capacity (q_t)
V_2O_5 -as	0.010	76.80	3787.50
	0.015	78.70	2587.50
	0.020	73.76	1818.70
	0.025	72.62	1432.50
	0.030	71.86	1181.20

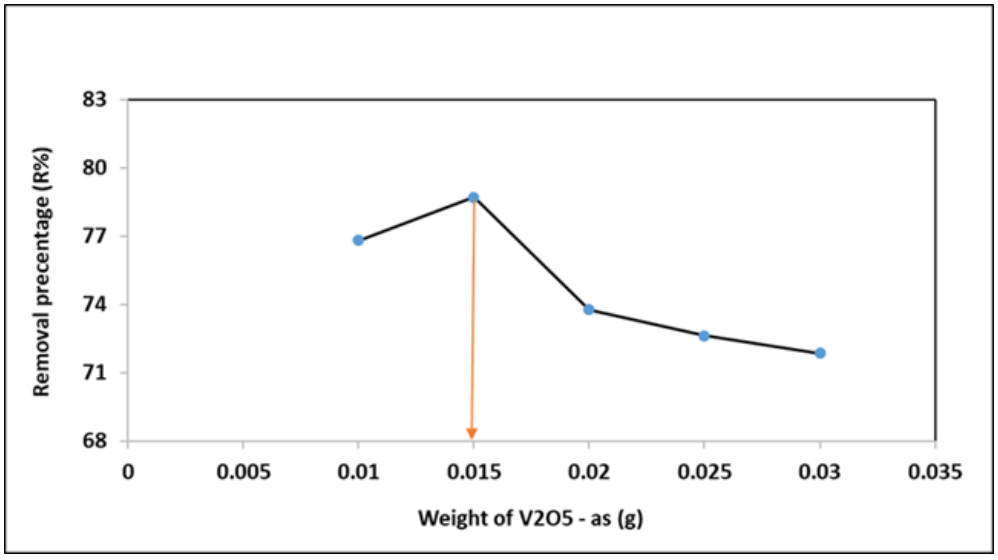

Figure 9: Effect of adsorbent weight on ninhydrin removal

The percentage of ninhydrin removal increased with the increase in the weight of the sorbent material. The maximum absorption (78.7 %R, 2587.5 q_t) was at a weight of 0.015 g when the other factors were the same. This is related to the fact that the more adsorption sites are available, the higher the ninhydrin removal.

B. The effect of ninhydrin concentration

The effect of concentration on the ninhydrin removal was studied by using (0.0908, 0.181, 0.2727, 0.363, 0.454,0.545, 0.636, and 0.727) mg/mL of ninhydrin was used to a fixed weight of $V_2O_5.nH_2O$ (0.015 g), ninhydrin concentration (0.2245 M), carbonate buffer (0.099 M), pH=10, shake speed (250 RPM), and shake time (15 min). Figure 10 and Table 6 summarize the findings.

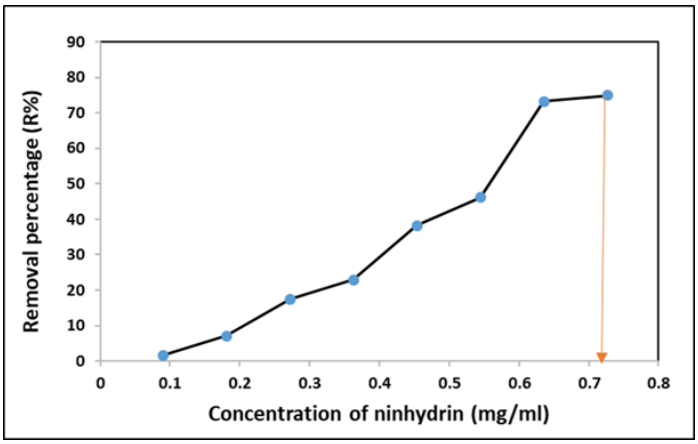

Figure 10: The impact of concentration on the removal of ninhydrin

Table 6: The values of percent removal (%R) and adsorption capacity (q_t) for the effect of ninhydrin concentration

	Concentration (mg/mL)	Percent removal (R %)	Adsorption capacity (q_t)
V_2O_5 -as	0.0908	1.69	6.10
	0.181	7.142	25.71
	0.2727	17.5	63.00
	0.363	22.88	82.37
	0.454	38.25	137.71
	0.545	46.19	166.30
	0.636	73.26	263.75
	0.727	74.915	269.69

The percentage of ninhydrin removal increased with the increase in the concentration of the ninhydrin, the maximum absorption (74.915 %R, 269.69 q_t) was at the concentration (0.727) mg/mL when the other factors were the same. The more adsorption sites are available, the higher the ninhydrin removal.

C. The effect of shake speed

The effect of shake speed on the ninhydrin removal was studied by using different shake speeds (50, 100, 150, 200, and 250) RPM to a fixed weight of $V_2O_5.nH_2O$ (0.015 g), ninhydrin concentration (0.727 mg/mL), ammonium hydroxide concentration (0.1122 M), carbonate buffer (0.099 M), pH=10, and shake time (15 min). Figure 11 and Table 7 represent the findings.

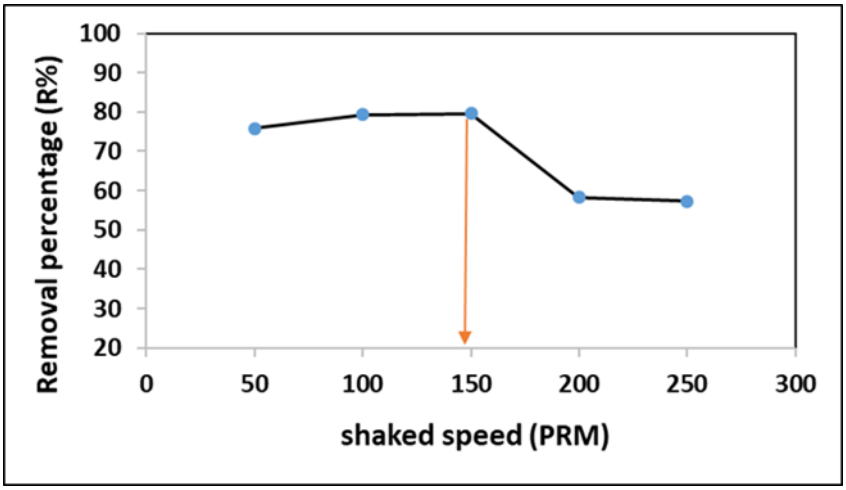

Figure 11: Effect of shake speed on ninhydrin removal

Table 7: The values of percent removal (%R) and adsorption capacity (q_t) for the effect of shaking speed

	Sake speed (PRM)	Percentage removal (%R)	Adsorption capacity (q_t)
V_2O_5	50	75.86	273.10
	100	79.31	285.51
	150	79.65	286.75
	200	58.27	209.79
	250	57.24	206.06

The percentage of ninhydrin removal increased with the increase in the shaking speed. The maximum absorption (79.655 %R, 286.758 q_t) was at shaking speed (150) RPM when the other factors were the same. This is related the more adsorption sites are available, the higher the ninhydrin removal.

D. The effect of shake time

The effect of shake time on the ninhydrin removal was studied by using different shake times (5, 10, 15, 20, and 25) min to a fixed weight of $V_2O_5.nH_2O$ (0.015 g), ninhydrin concentration (0.727 mg/mL), ammonium concentration (0.2245 M), carbonate buffer (0.099 M), pH=10, and shake speed (150 RPM). Figure 12 and Table 8 summarize the findings. The percentage of ninhydrin removal increased with the increase in the shaking time from (5 to 25) min. The maximum absorption (81.379 %R, 292.96 q_t) time is 10 min.

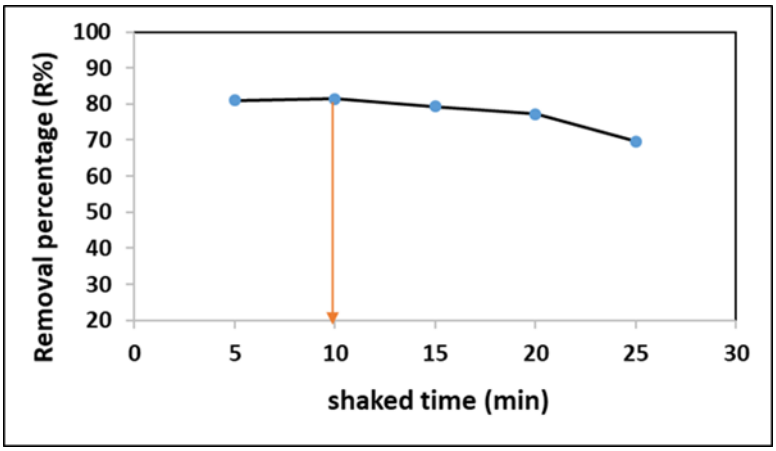

Figure 12. Effect of shake speed on ninhydrin removal

Table 8: The values of percentage removal (%R) and adsorption capacity (q_t) for the effect of shaking time

	Shake time(min)	Percentage removal (%R)	Adsorption capacity (q_t)
V_2O_5-as	5	81.03	291.72
	10	81.37	292.96
	15	79.31	285.51
	20	77.24	278.06
	25	69.65	250.75

Conclusion

In summary, we successfully prepared and characterized aluminum oxide (Al_2O_3) and vanadium pentoxide (V_2O_5) nanoparticles in hydrothermal process and heated at two temperatures (90 °C and 400°C). The ninhydrin removal was determined by Al_2O_3 and V_2O_5 nanoparticles. The results show that the (V_2O_5) nanoparticles had the greatest ninhydrin removal than the aluminum oxide especially the sample heated at 400 °C.

Acknowledgment

The Authors would like to express their appreciation to the Applied Science Department, University of Technology, Ministry of Higher

Education and Scientific Research, Baghdad, Iraq for supporting this work.

Funding

This research did not receive any specific grant from funding agencies in the public, commercial, or not-for-profit sectors.

Authors' contributions

All authors contributed to data analysis, drafting, and revising of the paper and agreed to be responsible for all the aspects of this work.

Conflict of Interest

The author declared that they have no conflict of interest.

ORCID:

Rashed T. Rasheed
https://orcid.org/0000-0002-7685-5377

References

[1]. Uddin M.J., Jeong Y.K., Urban river pollution in Bangladesh during last 40 years: potential public health and ecological risk, present policy, and future prospects toward smart water management, *Heliyon*, 2021, **7**:e06107 [Crossref], [Google Scholar], [Publisher]

[2]. Moghadam H.N., Banaei A., Bozorgian A., Biological Adsorption for Removal of Hydrogen Sulfide from Aqueous Solution by Live Eisenia Foetida Worms, *Advanced Journal of Chemistry, Section B: Natural Products and Medical Chemistry*, 2022, **4**:144 [Crossref], [Google Scholar], [Publisher]

[3]. Deletic A., Wang H., Water pollution control for sustainable development, *Engineering*, 2019, **5**:839 [Crossref], [Google Scholar], [Publisher]

[4]. Ajibade F.O., Adelodun B., Lasisi K.H., Fadare O.O., Ajibade T.F., Nwogwu N.A., Sulaymon I.D., Ugya A.Y., Wang H.C., Wang A., Environmental pollution and their socioeconomic impacts, *Microbe Mediated Remediation of Environmental Contaminants; Kumar, A., Singh, VK, Singh, P., Mishra, VK, Eds*, 2021, 321–354 [Crossref], [Google Scholar], [Publisher]

[5]. Abdullah T.A., Rasheed R.T., Juzsakova T., Al-Jammal N., Mallah M.A.P., Cuong L., Salman A.D., Domokos E., Ali Z., Cretescu I., Preparation and characterization of MnO2-based nanoparticles at different annealing temperatures and their application in dye removal from water, *International Journal of Environmental Science and Technology*, 2021, **18**:1499 [Crossref], [Google Scholar], [Publisher]

[6]. Ghanavati B., Bozorgian A., Esfeh H.K., Thermodynamic and Kinetic Study of Adsorption of Cobalt II using adsorbent of Magnesium Oxide Nanoparticles Deposited on Chitosan, *Progress in Chemical and Biochemical Research*, 2022, **5**:165 [Crossref], [Google Scholar], [Publisher]

[7]. Al-Senani G.M., Al-Fawzan F.F., Adsorption study of heavy metal ions from aqueous solution by nanoparticle of wild herbs, *The Egyptian Journal of Aquatic Research*, 2018, **44**:187 [Crossref], [Google Scholar], [Publisher]

[8]. Johnson A., Brous A., Samimi A., An Overview of the History of Using Adsorbents in Environment, *Advanced Journal of Chemistry-Section B: Natural Products and Medical Chemistry*, 2022, **4**:124 [Crossref], [Google Scholar], [Publisher]

[9]. Baig N., Kammakakam I., Falath W., Nanomaterials: A review of synthesis methods, properties, recent progress, and challenges, *Materials Advances*, 2021, **2**:1821 [Crossref], [Google Scholar], [Publisher]

[10]. Guerra F.D., Attia M.F., Whitehead D.C., Alexis F., Nanotechnology for environmental remediation: materials and applications, *Molecules*, 2018, **23**:1760 [Crossref], [Google Scholar], [Publisher]

[11]. Friedman M., Applications of the ninhydrin reaction for analysis of amino acids, peptides, and proteins to agricultural and biomedical sciences, *Journal of agricultural and food chemistry*, 2004, **52**:385 [Crossref], [Google Scholar], [Publisher]

[12]. Sreenivasan R.S., Kanagathara N., Ezhamani G., Renganathan N.G., Anbalagan G., Effect of Metal Dopant on Ninhydrin—Organic Nonlinear Optical Single Crystals, *Journal of Spectroscopy*, 2013, **2013**:386024 [Crossref], [Google Scholar], [Publisher]

[13]. Chen Y., Tang J., Wang S., Zhang L., Ninhydrin-functionalized chitosan for selective

removal of Pb (II) ions: characterization and adsorption performance, *International Journal of Biological Macromolecules*, 2021, **177**:29 [Crossref], [Google Scholar], [Publisher]

[14]. Das S., Recent applications of ninhydrin in multicomponent reactions, *RSC advances*, 2020, **10**:18875 [Crossref], [Google Scholar], [Publisher]

[15]. Kumar D., Rub M.A., Influence of dicationic quaternary ammonium gemini surfactant system on metal-amino acid complex-ninhydrin reaction, *Materials Chemistry and Physics*, 2020, **248**:122926 [Crossref], [Google Scholar], [Publisher]

[16]. Dani G.S., Djoko H.P., Jupiter S.P., Hydrothermally Synthesis of $A_{l2}O_3$ Nanoparticles for Nanofluids with Enhanced Critical Heat Flux, in *Journal of Physics: Conference Series*, 2020, **1428**:12023 [Crossref], [Google Scholar], [Publisher]

[17]. Nair D.P., Sakthivel T., Nivea R., Eshow J.S., Gunasekaran V., Effect of surfactants on electrochemical properties of vanadium-pentoxide nanoparticles synthesized via hydrothermal method, *Journal of Nanoscience and Nanotechnology*, 2015, **15**:4392 [Crossref], [Google Scholar], [Publisher]

[18]. Alshameri A., He H., Zhu J., Xi Y., Zhu R., Ma L., Tao Q., Adsorption of ammonium by different natural clay minerals: characterization, kinetics and adsorption isotherms, *Applied Clay Science*, 2018, **159**:83 [Crossref], [Google Scholar], [Publisher]

[19]. Bellahsen N., Varga G., Halyag N., Kertész S., Tombácz E., Hodúr C., Pomegranate peel as a new low-cost adsorbent for ammonium removal, *International Journal of Environmental Science and Technology*, 2021, **18**:711 [Crossref], [Google Scholar], [Publisher]

[20]. Hussain S.E., Naser J.A., Preparation and characterization of nickel oxide nanoparticles and its adsorption optimization for parachlorophenol, *Eurasian Chemical Communications*, 2022, **4**:1209 [Crossref], [Google Scholar], [Publisher]

[21]. Malaescu D., Grozescu I., Sfirloaga P., Vlazan P., Marin C.N., The Electrical Properties of Some Composite Materials Based on Sodium and Tantalum Oxides. *Acta Physica Polonica A*, 2016, **129**:133 [Google Scholar], [PDF]

[22]. Kim D., Jung J.H., Ihm J., Theoretical study of aluminum hydroxide as a hydrogen-bonded layered material, *Nanomaterials*, 2018, **8**:375 [Crossref], [Google Scholar], [Publisher]

[23]. Rasheed R.T., Mansoor H.S., Abdullah T.A., Juzsakova T., Al-Jammal N., Salman A.D., Al-Shaikhly R.R., Le P.C., Domokos E., Abdulla T.A., Synthesis, characterization of V2O5 nanoparticles and determination of catalase mimetic activity by new colorimetric method, *Journal of Thermal Analysis and Calorimetry*, 2021, **145**:297 [Crossref], [Google Scholar], [Publisher]

[24]. Haile H.L., Abi T., Tesfahun K., Synthesis, characterization and photocatalytic activity of $MnO_2/Al_2O_3/Fe_2O_3$ nanocomposite for degradation of malachite green, *African Journal of Pure and Applied Chemistry*, 2015, **9**:211 [Crossref], [Google Scholar], [Publisher]

[25]. Boumaza A., Favaro L., Lédion J., Sattonnay G., Brubach J.B., Berthet P., Huntz A.M., Roy P., Tétot R., Transition alumina phases induced by heat treatment of boehmite: an X-ray diffraction and infrared spectroscopy study, *Journal of solid state chemistry*, 2009, **182**:1171 [Crossref], [Google Scholar], [Publisher]

[26]. Toledo R.R., Santoyo V.R., Moncada D., Martínez M., Effect of aluminum precursor on physicochemical properties of $A_{l2}O_3$ by hydrolysis / precipitation method *Nova scientia,* 2018, **10**:83 [Crossref], [Google Scholar]

[27]. Djebaili K., Mekhalif Z., Boumaza A., Djelloul A.X.P.S., XPS, FTIR, EDX, and XRD analysis of $A_{l2}O_3$ scales grown on PM2000 alloy. *Journal of spectroscopy*, 2015, **2015** [Crossref], [Google Scholar], [Publisher]

[28]. Abdullah T.A., Juzsakova T., Rasheed R.T., Salman A.D., Adelikhah M., Cretescu I., V_2O_5 Nanoparticles for dyes removal from water. 2021 [Google Scholar]

[29]. Li Z., Cai J., Cizek P., Niu H., Du Y., Lin T., A self-supported, flexible, binder-free pseudo-supercapacitor electrode material with high capacitance and cycling stability from hollow, capsular polypyrrole fibers, *Journal of Materials Chemistry A*, 2015, **3**:16162 [Crossref], [Google Scholar], [Publisher]

[30]. Wu Y., Gao G., Wu G., Self-assembled three-dimensional hierarchical porous V2O5/graphene

hybrid aerogels for supercapacitors with high energy density and long cycle life, *Journal of Materials Chemistry A*, 2015, **3**:1828 [Crossref], [Google Scholar], [Publisher]

[31]. Fang B., Bao Z., Lu L., Zhao L., Wang H., Preparation of a hierarchical flower-like γ-Al_2O_3@C composite exhibiting enhanced adsorption performance for congo red by high temperature transformation of γ-AlOOH@ C precursors, *RSC advances*, 2016, **6**:61 [Crossref], [Google Scholar], [Publisher]

[32]. Mansour, S. F., Ahmed, M. A., El-Dek, S. I., Abdo, M. A., & Kora, H. H. (2017). Enhancement of the physical properties of novel (1− x) $NiFe_2O^{4+}$(x) Al_2O_3 nanocomposite, *Applied Physics A*, 2017, **123**:1 [Crossref], [Google Scholar], [Publisher]

[33]. Rahem S.A., Evaluation of fabricated IR absorbing films of polymer nanocapsules, *Eurasian Chemical Communications*, 2022, **4**:1228 [Crossref], [Google Scholar], [Publisher]

[34]. Baghdadi A.M., Saddiq A.A., Aissa A., Algamal Y., Khalil N.M., Structural refinement and antimicrobial activity of aluminum oxide nanoparticles, *Journal of the Ceramic Society of Japan*,, 2022, **130**:257 [Crossref], [Google Scholar], [Publisher]

[35]. Fu H.T., Zhang Z.K., Yang X.H., An X.Z., Two-step synthesis of V2O5 nanosheets with high sensing properties toward acetone. In *3rd Annual International Conference on Advanced Material Engineering (AME 2017)*, Atlantis Press, 2017, 372 [Crossref], [Google Scholar], [Publisher]

HOW TO CITE THIS ARTICLE

Zainab J. Abdul-Zahra, Rashed T. Rasheed. Preparation, characterization, and ninhydrin removal byAl2O3 and V2O5nanoparticles. *J. Med. Chem. Sci*., 2023, 6(2) 376-391

https://dx.doi.org/10.26655/JMCHEMSCI.2023.2.18

URL: http://www.jmchemsci.com/article_156295.html